CRBRP- GEFR-SP-139

DATE December 1978

# MASTER

CONF-781202--41

TITLE: INTERNAL FLUID FLOW MANAGEMENT ANALYSIS FOR CLINCH RIVER BREEDER REACTOR PLANT SODIUM PUMPS

AUTHORS: S. M. Cho, H. L. Zury, M. E. Cook and C. E. Fair

Prepared for publication in

1978 ASME Winter Meeting



This paper contains material resulting from work performed for: Westinghouse

Under Contract No. 54-7A0-192908BP & 54-7A0-192909BP

Under DA _____ task



GENERAL ELECTRIC

ADVANCED REACTOR SYSTEMS DEPARTMENT

SUNNYVALE, CALIFORNIA

# INTERNAL FLUID FLOW MANAGEMENT ANALYSIS FOR CLINCH RIVER BREEDER REACTOR PLANT SODIUM PUMPS

S. M. Cho[1] and H. L. Zury[2]

Nuclear and Advanced Technology Operations

Foster Wheeler Energy Corporation, Livingston, New Jersey

and

M. E. Cook[3] and C. E. Fair[4]

Byron Jackson Pump Division

Borg-Warner Corporation, Los Angeles, California

## ABSTRACT

The Clinch River Breeder Reactor Plant (CRBRP) sodium pumps are currently being designed and the prototype unit is being fabricated. In the design of these large-scale pumps for elevated temperature Liquid Metal Fast Breeder Reactor (LMFBR) service, one major design consideration is the response of the critical parts to severe thermal transients. Therefore, the key ingredients in the overall design/development program include tasks to assure adequate performance as well as reliable operation. In order to demonstrate sufficient margin for operability (i.e., against bearing seizure), a detailed thermal/structural analysis of the critical parts of the pump is required. To this end, a detailed internal fluid flow distribution analysis has been performed using a computer code HAFMAT, which solves a network of fluid flow paths. The results of the analytical approach are then compared to the test data obtained on a half-scale pump model which was tested in water. This paper presents the details of pump internal hydraulic analysis, and test and evaluation of the half-scale model test results.

---

(1) Manager, Thermal/Hydraulic & Systems Engineering, Mem. ASME
(2) Thermal/Hydraulic Engineer
(3) Manager of Design
(4) Technical Administrator for Nuclear Pumps

## INTRODUCTION

The Clinch River Breeder Reactor Plant (CRBRP) employs two sodium flow circuits for primary and intermediate sodium in each of three heat transport loops. The sodium flow is maintained by a pump which is located on the hot leg piping in the primary circuit or on the cold leg piping in the intermediate circuit, and these pumps are known as the primary and intermediate coolant pumps, respectively. Both primary and intermediate pumps are structurally identical to each other except that in the primary pump there are additional nozzles connected to the upper region of the pump tank for its unique functional requirements.

The CRBRP pumps are of the centrifugal type with two hydrostatic bearings straddling the impeller and, as such, proper internal fluid flow management and control (e. g., adequately maintaining the bearing flow) is essential for normal performance of the pumps. It is also noted that these pumps are designed per the rules of ASME Boiler & Pressure Vessel Code, Section III, Class 1 Components, and therefore, a detailed thermal/structural analysis is required to insure pump operability under various transient conditions. Of particular importance is operability against bearing seizure as a result of a severe thermal transient. To this end, appropriate internal fluid flow management and control must be provided in the critical parts of the pump internals in such a way that the temporal variations of structural temperatures neither impair pump operability nor jeopardize structural integrity of the pump.

This paper presents the analytical approach employed for the determination of internal fluid flow distribution. The results of the analysis are compared

to the experimental data obtained on a half-scale pump model which was tested in water.

## DESCRIPTION OF PROTOTYPE PUMP

Both primary and intermediate coolant pumps maintain geometrically as much commonality as possible. Hence the description of the prototype pump is directed toward the primary pump. The schematic of the primary pump is shown in Figure 1. It is a vertical single-stage, centrifugal pump. The pump casing contains three volute openings with a triple volute configuration and the impeller is of the double suction type with full suction flow around the inside of the pump tank. This arrangement is adopted to improve hydraulic and structural symmetry in the pump case which provides two-sided thermal shock to pump volute case, thereby resulting in minimum thermal distortions and stresses. The centerline of the pump shaft is 10.2 cm (4 in.) off the centerline of the lower tank sphere, the offset being 180° away from the suction nozzle, to provide better suction flow distribution into the impeller. (Note that this inlet configuration was tested using air in a $\frac{1}{4}$-scale model). Nozzle configuration is side suction and side discharge, 90° apart. There are two hydrostatic bearings straddling the impeller. The principal considerations which led to the selection of two bearings are (1) reduction in size and weight of the pump and pump shaft increasing the reliability under high temperature service, (2) reduced bearing diameters and a decrease in leakage, and at the same time allowing for more bearing-to-journal clearance, and (3) higher confidence in dynamic analysis because of reduction in shaft size. A pressure balance port (not shown in Figure 1) is located opposite to the discharge opening in the hydraulic assembly, to counter-balance the effect of high-pressure fluid discharging out of the hydraulic aseembly. The pump has a tapered adjustable static seal to keep the leakage flow from discharge to suction down to a

minimum. The driver is a vertical oil-filled variable speed motor.

The design is based upon the free surface centrifugal pump concept, similar to Fermi & Hallam pumps. There is a buffer cover gas contained between the liquid sodium surface and the oil lubricated mechanical shaft seal. The level of the liquid sodium surface in the primary pump tank is established and controlled by a standpipe bubbler system, and is normally maintained at 2.44m (8 ft) below the normal reactor sodium level. A continuous flow of inert gas is supplied to the pump cover gas space. The gas supply pressure will be sufficient to depress the liquid sodium level to the standpipe nozzle and the gas will bubble up the standpipe to the reactor cover gas system. The primary pump contains radiation as well as thermal shields in the upper tank internal. Also for the primary pump, there is a continuous vent flow from the intermediate heat exchanger (IHX) into the upper tank.

Table 1 delineates the steady-state, full load operating conditions for the CRBRP pumps. It is noted that the flowrates and total developed heads specified in the table are the quantities delivered to the respective flow circuits external to the pumps and differ slightly from the equivalent values through the impellers. In other words, the impellers develop slightly higher head differentials at higher flow rates, and the differences are primarily due to pump internal pressure drops and various internal secondary flows. The internal secondary flow paths that are important to the design are as follows:

(1) Hydrostatic bearing flow - The high-pressure discharge flow in the pump casing is ducted into sixteen bearing pockets (eight in each of the upper and lower bearings) and discharged into the lower pump tank below the impedance plate and the suction duct through the clearance between the bearing pockets

Table 1 CRBRP Pump Steady-State Operating Conditions

| | Primary Pump | Intermediate Pump |
|---|---|---|
| Weight flow rate, kg/sec (lb/sec) | 1741 (3839) | 1610 (3550) |
| Volumetric flow rate, $m^3$/sec (gpm) | 2.126 (33,700) | 1.861 (29,500) |
| Total developed head, m (ft) | 139.6 (458) | 103.3 (339) |
| Fluid temperature, °C (°F) | 535 (995) | 344 (651) |
| Shaft speed, rpm | 1116 | 1116 |
| Total suction pressure available, m (ft) of sodium at inlet temperature | 16.2 (53) | 93.0 (305) |
| Cover gas pressure, kPa-gage (psig) | 2.48 (0.36) | 793 (115) |

and the bearing journals. The maintenance of this clearance at all times is of paramount importance because complete closure of the clearance may lead to bearing seizure.

(2) Bearing journal flow - The bearing journals contain flow holes and the flow direction is from the tank to the suction side of the impeller for the design shown in Figure 1. The journal flow tends to reduce the temperature difference between the journal and the bearing pocket so that the journal-to-bearing clearance is maintained.

(3) Internal impedance path - This is a controlled leakage flow between the lower and upper tank through the impedance plate. The prime function of this impedance is to provide throttling of the flow into and out of the upper pump tank during a plant trip. When the pump is tripped, the suction line hydraulic flow loss decreases, causing an increase in pump suction head. This increase in pump suction head produces a flow into the upper pump tank and a volumetrically identical drop in the reactor vessel sodium level. The inertia of the moving sodium produces an overshoot in both vessels. This results in a damped oscillation of fluid levels in the pump tank and the reactor vessel. This condition is further complicated by the concurrent reactor scram which results in a rapid temperature drop and a large shrinkage of the sodium volume, producing an additional drop in the reactor liquid level. The combination of the three pumps with the reactor vessel under these conditions results in nine degrees of freedom for oscillation of the liquid level between these vessels during the trip transient. Therefore, it is necessary to size the pump tank internal impedance to limit the fluid level excursion in the reactor vessel. The standpipe bubbler level controller will limit the liquid level fluctuations

within the respective pump tanks.

(4) Leakage from the discharge nozzle - This is a leakage flow from the discharge nozzle and the pressure balance port to the lower pump tank through the clearance gap between the sealing cone and the hydraulic assembly. This leakage flow should be minimized because it contributes to the degradation of the pump hydraulic efficiency.

(5) IHX vent return flow - There is a continuous vent flow from the intermediate heat exchanger into the pump. In the initial design, the IHX vent fluid entered the lower pump tank through a nozzle located in the bottom of the tank, flowed up the inside of the shaft and discharged into the upper pump tank just above the bearing shroud. However, this flow configuration has contributed to a substantial temperature differential between the shaft/journals and the bearing pockets as a result of the time delay of the returning IHX sodium. In the revised design, the IHX vent return flow is routed into the upper pump tank.

(6) Bearing pocket web flow - There are flow holes in the bearing pocket webbing and the flow through these holes provide proper thermal tracking between the webs and the remainder of the bearing housing.

(7) Various internal flow streams are hydraulically as well as thermally mixed at various junction locations and the resulting thermal-hydraulic conditions are imposed downstream.

The internal flow paths and mixing processes described above are further discussed in the next section.

## INTERNAL FLOW DISTRIBUTION ANALYSIS METHOD

The internal fluid flow paths of the prototype pump are shown in Figure 2.

The main sodium flow path is designated by the large arrows and the small arrows indicate some of the secondary flow paths. The corresponding flow network is shown in Figure 3. In this figure, the numerals indicate flow paths or flow branches and the letters designate flow junctions or nodes. A complete description of all the internal flow paths is given in Table 2. The flow path number designation in the table corresponds to the same path number shown in Figure 3.

The flow network diagram of Figure 3 shows the interrelation of all the internal fluid flow paths. This fluid flow network is similar to an electrical network consisting of resistances connected in series and parallel. Because of the interaction of the flow paths the system must be considered as a whole. Any change in one flow path will have some effect on all the other flow paths.

The basic method of solution to the above flow network consists of writing the pressure drop versus flowrate relationship along each flow path and the mass conservation equation at each node or junction point, and then solving the resulting equations simultaneously using a computer code called HAFMAT. *

The HAFMAT computer code calculates the steady state distribution of flow to all paths of a given flow system. The flow geometry is specified for each flow path and the system is bounded by specifying inlet and outlet boundary conditions. The system is broken into a finite number of flow paths which account for all of the fluid volume. The flow paths in the network are called branches and the junctions of flow paths are referred to as nodes. Each branch has an inlet and outlet node at which perfect mixing of flows from two or more branches is assumed to occur. Nodes do not have any flow capacity and are described in terms of static pressure.

---

* Wunderlich, L. H., and Dolk, D. R., "HAFMAT-Steady State Flow Distribution Program," General Electric Report KAPL-M-7128 (1970)

Table 2

Flow Network Description

| Flow Path Number | Description |
|---|---|
| 1 | Flow In Pump Suction To Impeller Eye Through Inlet Webbing |
| 2 | Flow Through Impeller |
| 3 | Flow In First Half Of Volute |
| 4 | Flow In Second Half Of Volute |
| 5 | Volute Outlet Flow |
| 6 | Discharge Nozzle Flow |
| 7 | Flow In Upper Bearing Pocket Orifice Feed Lines |
| 8 | Flow In Lower Bearing Pocket Orifice Feed Lines |
| 9 | Upper Bearing Pocket Leakage Flow Through Journal-Bearing Clearance And Bearing Drain Grooves Into Upper Chamber |
| 10 | Lower Bearing Pocket Leakage Flow Through Journal-Bearing Clearance And Bearing Drain Grooves Into Lower Tank |
| 11 | Flow Through Lower Journal Inlet Holes |
| 12 | Flow Through Lower Journal Outlet Holes |
| 13 | Flow Through Upper Journal Inlet Holes |
| 14 | Flow Through Upper Journal Outlet Holes |
| 15 | Upper Bearing Pocket Leakage Flow Through Journal-Bearing Clearance Into Impeller Eye |
| 16 | Lower Bearing Pocket Leakage Flow Through Journal-Bearing Clearance Into Impeller Eye |
| 17 | Flow Through Bearing Shaft Annulus |
| 18 | Flow Through Interstructure (Impedence Plate) Annulus From Upper Tank To Lower Tank |
| 19 | Leakage Flow From Volute To Impeller Eye Through Gap Between Upper Static Shroud And Pump Case |

Table 2 (cont'd)

Flow Network Description

| Flow Path Number | Description |
|---|---|
| 20 | Leakage Flow From Discharge To Lower Tank Through Gap Between Sealing Cone And Pump Case At Discharge Nozzle |
| 21 | Discharge Nozzle Leakage Flow |
| 22 | Flow Through Holes From Upper Chamber To Lower Tank |
| 23 | Flow Through Holes In Upper Bearing Webbing |
| 24 | Flow Through Holes In Lower Bearing Webbing |
| 25 | Flow Through Holes In Lower Bearing Webbing |
| 26 | Leakage Flow From Volute To Lower Tank Through Gap Between Sealing Cone And Pump Case At Balance Port |
| 27 | Flow Through Balance Port Hole |
| 28 | Leakage Flow In Gap Between Gudgeon And Support Post |
| 29 | Leakage Flow Inside Support Post |
| 30 | Flow Through Drain Holes In Support Post |
| 31 | IHX Vent Return Inlet Flow To Upper Tank |
| 32 | Inlet Nozzle Flow |

The network inlet boundary points, specifically the pump suction and the IHX vent line inlet, are input as fixed flow rates. The outlet boundary point, the pump discharge, is fixed at the discharge static pressure. The code has a pump head option which is used to simulate the head rise which occurs at the pump impeller. For this branch of the network, a table is input which contains the pump head rise as a function of sodium flow in the impeller.

The program assumes an initial flow distribution consistent with the inlet flow rates using a set of linear nodal flow summation equations. This set of equations is constructed so that the sum of all flows entering a node is divided among all the branches exiting that node, initially in proportion to their flow areas. This initial flow distribution is then used in conjunction with geometry specifications to calculate the static pressure drop from the inlet to the outlet of each branch.

Each branch of the flow network is described with a corresponding flow area and hydraulic loss coefficient for the purpose of calculating the pressure drop between nodes using the following equation:

$$\Delta P = \bar{K} \frac{1}{2 g_c \rho} \left( \frac{W}{A} \right)^2$$

where $\Delta P$ is branch pressure drop, $\bar{K}$ total hydraulic loss coefficient, W branch flow rate, $g_c$ gravitational constant, $\rho$ fluid density, and A flow area.

The total hydraulic loss coefficient is given by:

$$\bar{K} = \frac{f L}{d_H} + \Sigma K$$

where f is friction factor, L flow path length, $d_H$ hydraulic diameter, and $\Sigma K$ = summation of path loss coefficients due to area contraction, expansion, turns, etc. Important loss coefficients used for the flow paths are K = 1.0 for sudden area expansion, K = 0.5 for sudden area contraction, and K = 2.0 for bearing orifice; all based on the minimum flow area.

After the pressure drop has been calculated for each branch, a matrix technique is used to determine the static pressure at each node, based on the branch pressure drops and node mass conservations. The difference in pressures for the two nodes at opposite end of each branch is compared with the calculated pressure drop for the branch. This difference is used to readjust the amount of flow for that branch. Pressure drops are then recalculated based on the new flow distribution, a new set of junction pressure mismatches are produced, and this iterative process continues until the deviations are minimized and convergence is obtained.

## FLOW DISTRIBUTION RESULTS FOR PROTOTYPE PUMP

The HAFMAT flow distribution code described above was run for various CRBRP pump flow conditions. The results for the primary pump operating at full load are presented in Tables 3 and 4 in terms of the branch flow and junction pressure, respectively. The impeller outputs a flowrate of 1878 kg/sec (Branch No. 2), of which 1750 kg/sec (Branch No. 6) is delivered to the external sodium circuit. The total bearing flowrate is 75.8 kg/sec (Branch No. 7 and No. 8).

The fluid flow rates obtained in the HAFMAT analysis of the fluid flow network were applied directly in the thermal analysis at the pump to verify its

Table 3

Internal Flow Distribution For The Prototype Pump - Full Load

| Flow Path or Branch No. | Flow kg/sec (lb/sec) | Flow Path or Branch No. | Flow kg/sec (lb/sec) |
|---|---|---|---|
| 1 | 1808 (3987) | 17 | 5.08 (11.2) |
| 2 | 1878 (4140) | 18 | 15.6 (34.4) |
| 3 | 1878 (4140) | 19 | 4.01 (8.84) |
| 4 | 1775 (3913) | 20 | 22.8 (50.3) |
| 5 | 1752 (3863) | 21 | 1.82 (4.02) |
| 6 | 1750 (3859) | 22 | 3.30 (7.28) |
| 7 | 37.8 (83.4) | 23 | 8.35 (18.4) |
| 8 | 38.0 (83.8) | 24 | 17.3 (38.1) |
| 9 | 25.5 (56.2) | 251 | 17.3 (38.1) |
| 10 | 25.9 (57.0) | 26 | 16.4 (36.1) |
| 11 | 6.40 (14.1) | 27 | 6.58 (14.5) |
| 12 | 6.40 (14.1) | 28 | 1.62 (3.57) |
| 13 | 8.75 (19.3) | 29 | 4.94 (10.9) |
| 14 | 8.75 (19.3) | 30 | 4.94 (10.9) |
| 15 | 12.3 (27.2) | 31 | 10.4 (22.9) |
| 16 | 12.2 (26.9) | 32 | 1740 (3836.) |

Table 4

Internal Pressure Distribution For The Prototype Pump - Full Load

| Node | Pressure MPa (Psi) | Node | Pressure MPa (Psi) |
|---|---|---|---|
| A | 0.136 (19.7) | J | 0.139 (20.2) |
| B | 0.117 (17.0) | K | 0.134 (19.5) |
| C | 1.27 (183.6) | L | 0.127 (18.4) |
| D | 1.27 (183.6) | M | 0.127 (18.4) |
| E | 1.24 (180) | N | 1.27 (183.6) |
| F | 1.24 (180) | O | 1.27 (183.6) |
| G | 0.453 (65.7) | P | 0.136 (19.7) |
| H | 0.445 (64.5) | Q | 0.175 (25.4) |
| I | 0.152 (22.1) | | |

structural integrity under various thermal transient conditions. To this end, a thermal model of the pump was constructed using a multi-dimensional, general-purpose finite difference heat transfer computer code called SINDA*. In this model, the entire pump, including the sodium flow paths, is divided into a number of thermal elements and energy conservation equations are written for each element. The resulting equations are solved simultaneously, using the SINDA program, to obtain transient temperatures at all elements. The fluid transient temperature variations for selected internal flow paths of the primary pump during uncontrolled rod withdrawal from full power are shown in Figure 4, for illustration purpose.

The thermal and hydraulic conditions obtained from the SINDA and HAFMAT models are used to provide the boundary conditions for thermal structural analysis of the various pump components.

## FLOW MODEL TEST AND EVALUATION

A hydraulic scale model water test was conducted, primarily to verify the overall hydraulic performance characteristics of the pump. The limited instrumentation contained in the test model enables one to compare the analytical prediction of internal flow distribution with the experimental indications. The test and evaluation of this model test program, as it applies to the validation of the analytical method, is discussed herein.

The hydraulic test article is a one half scale model of the prototype pump, and as such, it is geometrically similar to the full size unit except that it reflects an earlier version of the pump design. The internal configuration of

* SINDA - System Improved Numerical Differencing Analyzer Computer Code, Modified 3G version, Foster Wheeler Energy Corporation Report ND-75-71 (1976)

the test model is shown in Figure 5. Since the construction of the test model, the design has undergone a few revisions which can be noted by comparing Figure 5 with Figure 2. The major differences are the ducted suction flow configuration and the shaft centerline being placed at the centerline of the pump tank in the test model. The validity of the scale model test is not affected by these changes in configuration. Pressure taps are located in the test model to measure bearing pocket pressures (all 16 pockets), pump tank cavity pressures (4 locations), bearing pocket supply pressures (4 locations), and also suction pressure to the impeller. Some of these pressure tap locations are shown in Figure 5.

Figure 6 shows the schematic of the pump test circuit in the Byron-Jackson Pump Division Hydraulic Laboratory at Vernon, California. The test model was mounted vertically and driven by an oil filled variable speed electric motor. The variable speed system consisted of a generator, eddy current coupling and an electric motor. The test loop consisted of a 400,000 gallon open pit, a suction booster, a venturi in the suction line, a suction flow control valve, a suction bypass line and a discharge pipe with a flow control valve. Water was drawn from the open pit through the booster pump, through the venturi, to the hydraulic scale model, through the discharge valve and returned to the pit. Suction and discharge gages were properly installed and located to measure the developed pressure head. The venturi was sized for the anticipated test flow range.

Three series of tests were conducted. In the first series, the leakage flow from the bearings and the discharge nozzle was allowed to drain from the bottom of the spherical lower tank. A sump pump was installed in the drain line which received the leakage from the spherical tank and discharged it through a venturi flowmeter into the pit. In the second series of tests, a bypass line was installed from the bottom of the lower tank to the standing

water in the upper tank. The leakage was thereby returned to the internal fluid system and not measured as in the first series. In both first and second series, all sixteen bearing pocket pressures were measured. The third series of tests were conducted with additional pressure probes installed in the lower tank and the volute for the purpose of measuring the internal pressure distribution in more detail. This test used the bypass line as the second series.

The results of the three series of tests discussed above are presented in Tables 5, 6, 7 in terms of static pressures and leakage flow rates that were actually measured. The measured pressures shown in the tables are the average values in their respective locations. In order to compare these results with those of the analytical method used in the prototype pump analysis, a HAFMAT flow network model, similar to Figure 3, was constructed of the test model internal flow paths, and the results are also shown in these tables.

For the first series of tests (Table 5), the predicted bearing pressures are very close to the measured values while the measured leakage rates are somewhat greater than the predicted values. The latter is partly due to the presence of a sump pump in the drain line which was not simulated in the HAFMAT model. For the second series of tests in which only bearing pocket pressures were measured, the predicted bearing pressures are slightly higher than the measured pressures (Table 6). In order to obtain the internal pressure distribution in more detail, and thus to reduce the analysis uncertainties, additional pressure probes were installed for the third series of tests, as mentioned earlier. The results shown in Table 7 indicate rather close agreement between measured and predicted values. It is noted that the flow rates of internal flow streams cannot be measured directly because the presence of any probes in these narrow flow paths would affect the entire flow network.

Table 5 Results of Test Series 1

| Flow Rate $m^3/sec$ | Pump Speed rpm | Bearing Pressure MPa-gage | | Leakage Flow $m^3/sec$ | |
|---|---|---|---|---|---|
| | | Measured | Predicted | Measured | Predicted |
| 0.3817 | 1769 | 0.359 | 0.357 | 0.0271 | 0.0239 |
| 0.4290 | 1778 | 0.334 | 0.326 | 0.0240 | 0.0229 |
| 0.4779 | 1781 | 0.315 | 0.301 | 0.0231 | 0.0220 |
| 0.5186 | 1786 | 0.267 | 0.224 | 0.0186 | 0.0189 |
| 0.3085 | 1782 | 0.385 | 0.379 | 0.0276 | 0.0247 |
| 0.1593 | 1783 | 0.427 | 0.423 | 0.0287 | 0.0261 |
| 0.4984 | 1776 | 0.320 | 0.301 | 0.0245 | 0.0220 |
| 0.4208 | 1786 | 0.368 | 0.361 | 0.0249 | 0.0240 |

Table 6 Results of Test Series 2

| Flow Rate $m^3/sec$ | Pump Speed rpm | Bearing Pressure MPa-gage | |
|---|---|---|---|
| | | Measured | Predicted |
| 0.2839 | 1985 | 0.554 | 0.645 |
| 0.3388 | 1985 | 0.503 | 0.597 |
| 0.3975 | 1985 | 0.451 | 0.492 |
| 0.4574 | 1985 | 0.401 | 0.505 |
| 0.5129 | 1985 | 0.340 | 0.410 |
| 0.5716 | 1985 | 0.320 | 0.326 |

Table 7

Results of Test Series 3

| Flow Rate $m^3/sec$ | Pump Speed rpm | Bearing Pressure MPa-gage | | Volute Pressure MPa-gage | | Lower Tank Pressure MPa-gage | |
|---|---|---|---|---|---|---|---|
| | | Measured | Predicted | Measured | Predicted | Measured | Predicted |
| 0.4240 | 1785 | 0.259 | .320 | 0.888 | 0.909 | 0.028 | 0.038 |
| 0.3331 | 1400 | 0.174 | .207 | 0.574 | 0.576 | 0.033 | 0.029 |
| 0.2858 | 1190 | 0.142 | .162 | 0.431 | 0.431 | 0.041 | 0.034 |
| 0.1893 | 795 | 0.0917 | .0986 | 0.221 | 0.224 | 0.038 | 0.039 |

## CONCLUSIONS

The internal fluid flow distribution analysis for CRBRP sodium pumps is presented. The analysis utilizes a network of various internal flow paths, and the flow network is solved iteratively using a computer code HAFMAT. The analytical predictions are compared with limited experimental data obtained in a half-scale model test in water. The predicted and measured values are generally in good agreement, thus rendering a credence to the analytical method employed.

## ACKNOWLEDGEMENT

The authors wish to thank all members of the CRBRP pump design team at Borg-Warner Corporation and Foster Wheeler Energy Corporation for their contributions to the pump development. This paper is based on work which was supported by the U. S. Department of Energy through Borg-Warner Corporation Byron Jackson Pump Division under FWEC Contract No. 8-33-3011.

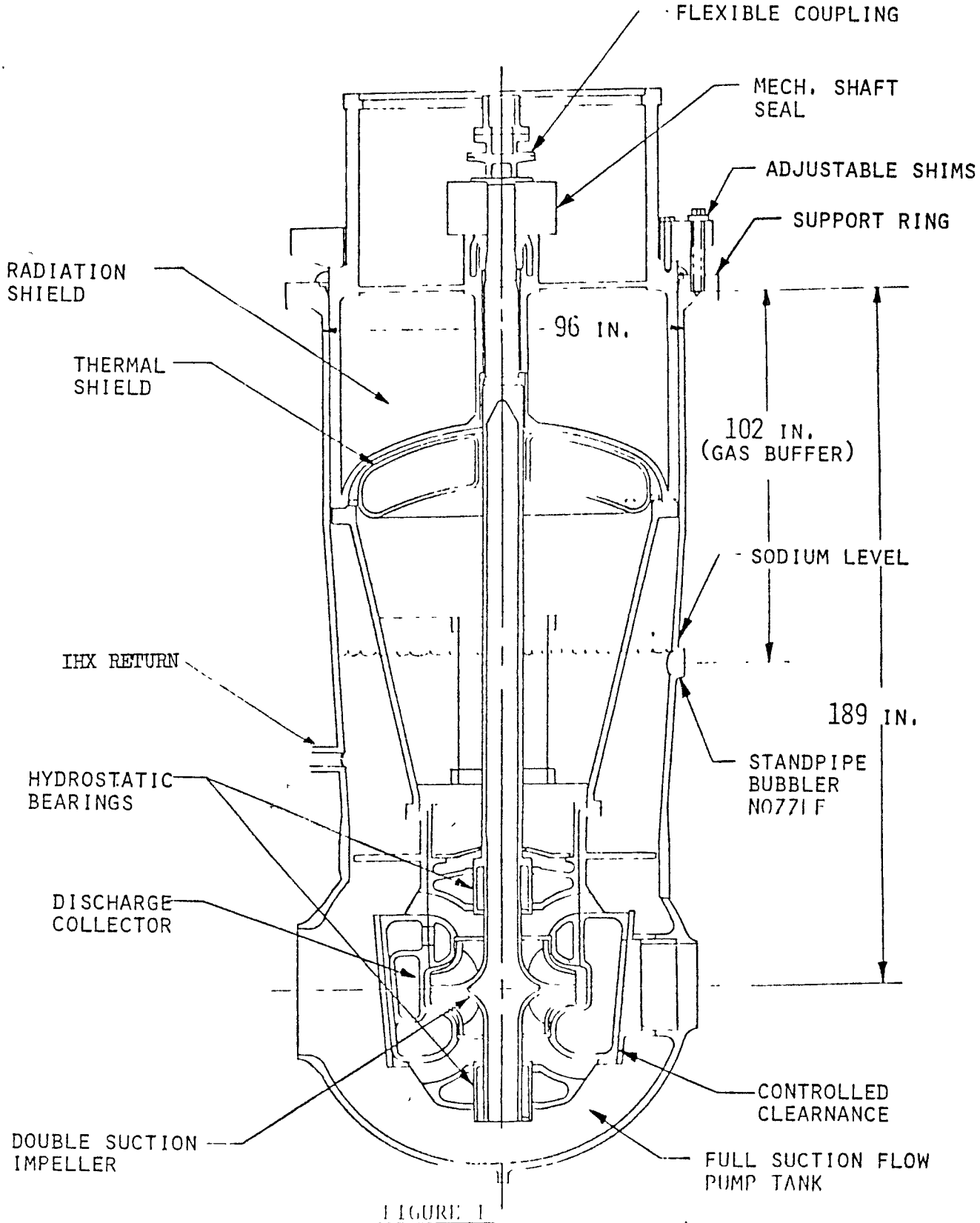


FIGURE 1
CRBRP PRIMARY PUMP

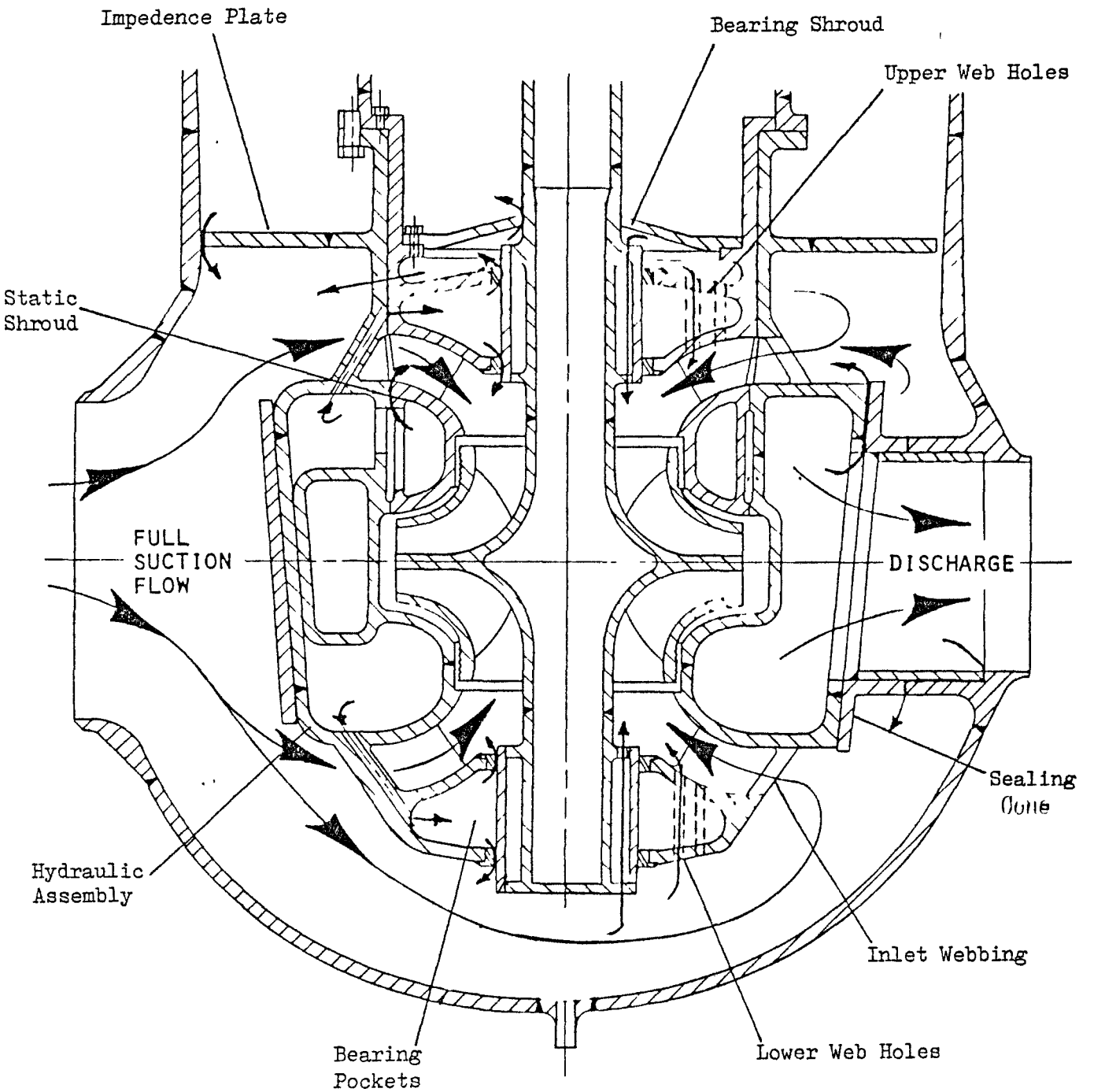


FIGURE 2

PROTOTYPE PUMP INTERNAL FLOW PATHS

FIGURE 3

FLOW NETWORK FOR THE PROTOTYPE PUMP

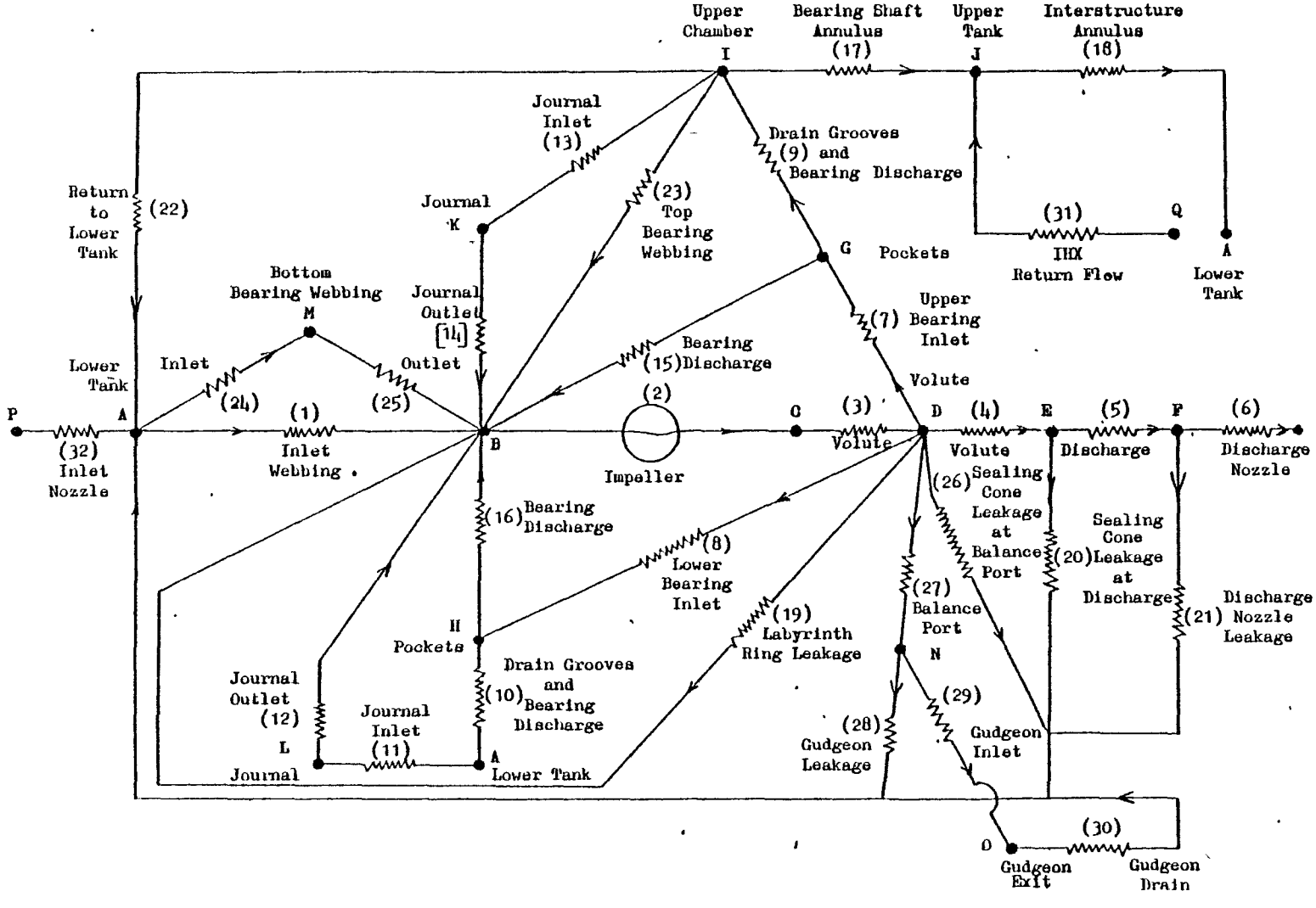

FIGURE 4

FLUID TEMPERATURE VARIATIONS FOR PRIMARY PUMP DURING UNCONTROLLED ROD WITHDRAWAL EVENT

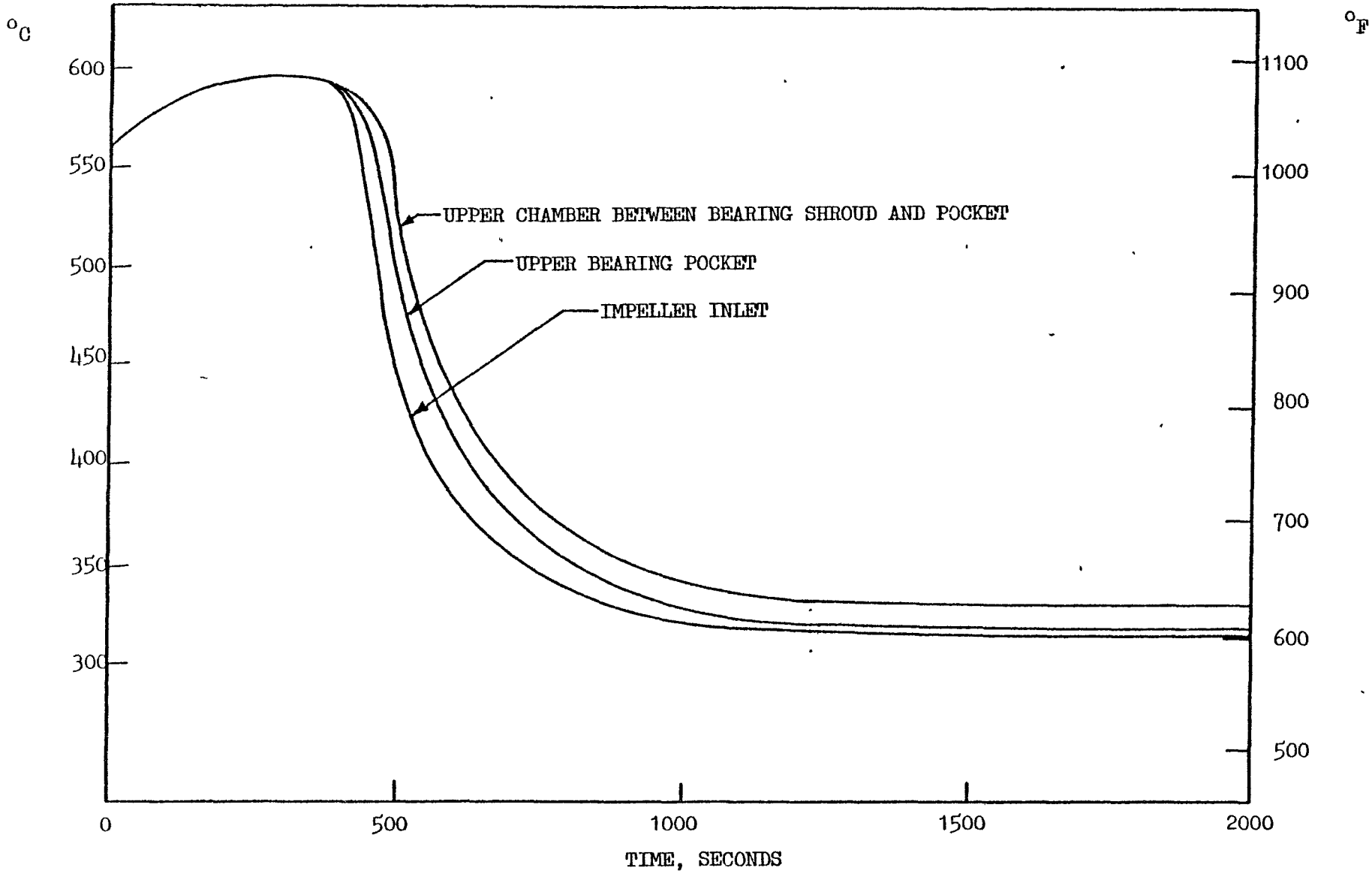

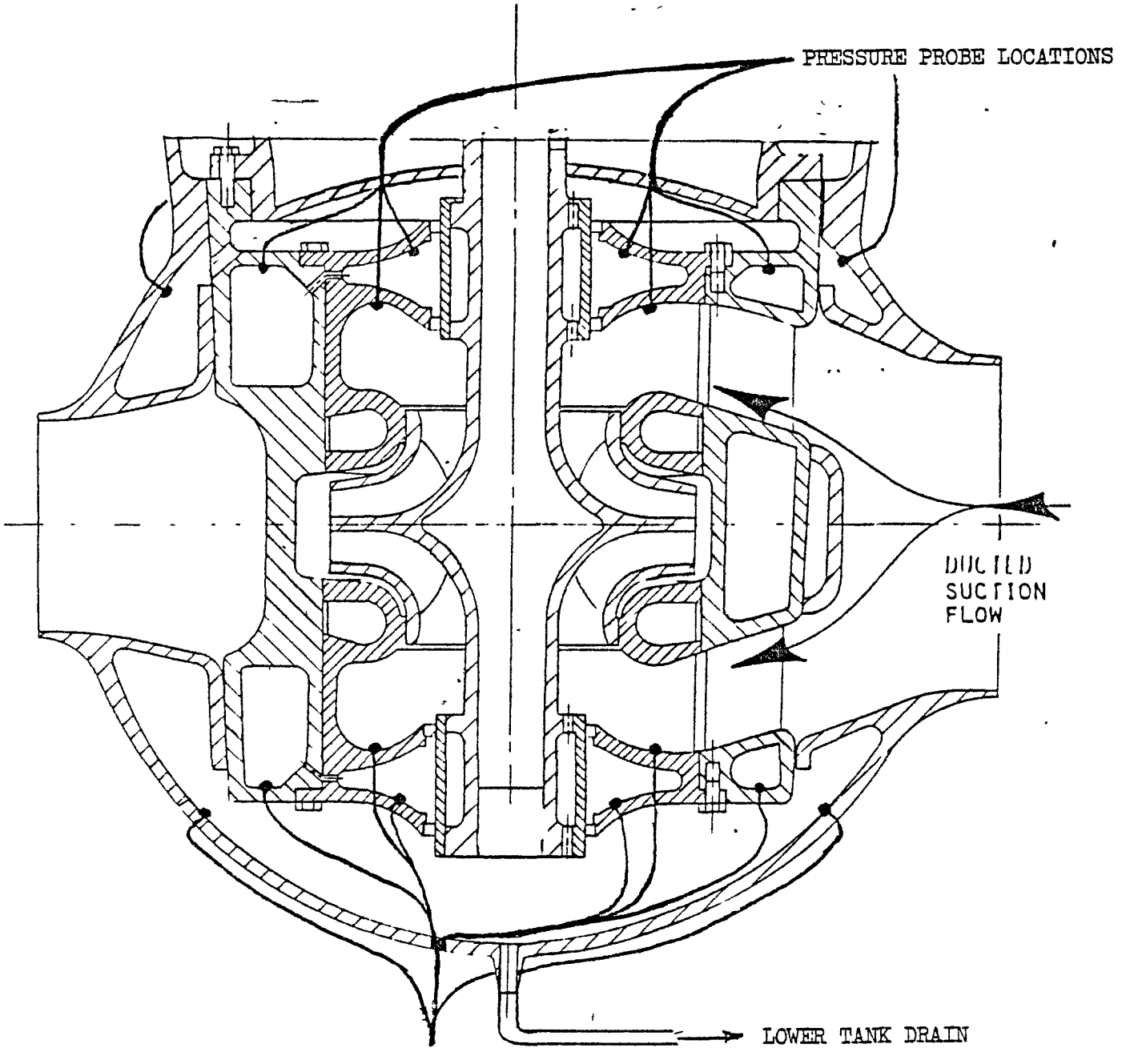


FIGURE 5

HALF SCALE TEST MODEL

FIGURE 6

SCHEMATIC OF THE PUMP TEST CIRCUIT